Pergamon

Geochimica et Cosmochimica Acta, Vol. 66, No. 16, pp. 2915–2928, 2002

0016-7037/02 $22.00 + .00

PII S0016-7037(02)00877-3

Water in peralkaline aluminosilicate melts to 2 GPa and 1400°C

BJORN MYSEN*

Geophysical Laboratory, Carnegie Institution of Washington, 5251 Broad Branch Road NW, Washington, DC 20015, USA

(*Received September* 21, 2001; *accepted in revised form February* 25, 2002)

Abstract—The solubility of H_2O in melts along the join $CaSi_4O_4$-$Ca(Ca_{0.5}Al)_4O_9$ (0, 3, and 6 mol% Al_2O_3) has been determined at 0.8 to 2.0 GPa and 1200 to 1400°C and compared with the solubility of H_2O in melts along the joins $Na_2Si_4O_9$-$Na_2(NaAl)_4O_9$ and $K_2Si_4O_9$-$K_2(KAl)_4O_9$. The H_2O solubility is a positive function of pressure and a negative function of temperature and Al_2O_3 content so that solubility, $X_{H_2O^{melt}}$ (mol%), is

$$X_{H_2O}^{melt}(CAS) = 19 \pm 2 - 0.7 \pm 0.1 \cdot X_{Al_2O_3} + 0.06 \pm 0.02 \cdot (X_{Al_2O_3})^2 + 13.3 \pm 0.2 \cdot P(GPa) - 0.011 \pm 0.001 \cdot T(K).$$

In alkali aluminosilicate melts, the solubility is considerably more sensitive to pressure, Al_2O_3, and temperature.The H_2O solubility data in the 0.8- to 2.0-GPa and 1200 to 1400°C pressure and temperature range are consistent with constant activity coefficient of H_2O in the melt. The partial molar volume of H_2O, $\bar{V}_{H_2O}^{melt}$, derived from the solubility data, ranges between 12.4 cm^3/mol for Al-free $CaSi_4O_9$ melt and 10.4 cm^3/mol for $CaSi_4O_9$ + 6 mol% Al_2O_3. This decrease in $\bar{V}_{H_2O}^{melt}$ with increasing Al_2O_3 is similar to that reported for H_2O in melts along the two alkali aluminosilicate joins ($Na_2Si_4O_9$-$Na_2(NaAl)_4O_9$ and $K_2Si_4O_9$-$K_2(KAl)_4O_9$). The $\bar{V}_{H_2O}^{melt}$ is invariant with temperature in contrast to $\bar{V}_{H_2O}^{melt}$ along the joins, $Na_2Si_4O_9$-$Na_2(NaAl)_4O_9$ and $K_2Si_4O_9$-$K_2(KAl)_4O_9$, where in both cases $\bar{V}_{H_2O}^{melt}$ decreases with increasing temperature. *Copyright © 2002 Elsevier Science Ltd*

1. INTRODUCTION

Igneous and hydrothermal processes in the Earth's interior are often affected by H_2O. The compositional trends of magmatic liquids during melting and crystallization are affected by water dissolved in the magma (e.g., Kushiro, 1972, 1990; Mysen and Boettcher, 1975; Gaetani et al., 1993), owing largely to reduction of silica activity in the magma upon solution of H_2O. Furthermore, melt viscosity is significantly lower than that of the anhydrous equivalents (Kushiro, 1978; Schulze et al., 1996; Dingwell et al., 1998; Holtz et al., 1999; Romano et al., 2001). The density of hydrous magma is lower than that of anhydrous melts (e.g., Kushiro, 1978; Richet and Polian, 1998; Mysen and Wheeler, 2000a). Volcanic eruption dynamics are in part controlled by the volume difference between H_2O in melt solution and in aqueous fluid (e.g., Eichelberger and Westrich, 1981; see also Woods, 1988, for review). Therefore, the dynamics of magma aggregation at depth, magma ascent, emplacement, and eruption depend on the water content of the magmatic liquid. Quantitative characterization of these properties requires, in part, knowledge of the solubility and solubility mechanisms of H_2O in silicate melts at high pressure and temperature.

There are a substantial amount of data on H_2O solubility and solubility mechanisms in magmatic liquids in the pressure regime of the Earth's crust (less than 1 GPa; see, e.g., Goranson, 1936; Hamilton et al., 1964; Hamilton and Oxtoby, 1986; McMillan et al., 1986; Dixon and Stolper, 1995; Nowak and Behrens, 1995; Shen and Keppler, 1995; Holtz et al., 1995, 1996; Carroll and Blank, 1997; Dingwell et al., 1997; Behrens and Cantos, 2001). Many igneous processes do, however, occur at higher pressures corresponding to those of the upper mantle. Solubility data in that pressure/temperature regime are less common. Experimental information exists for only a few simple system compositions such as SiO_2-H_2O (Boettcher, 1984), $CaMgSi_2O_6$-H_2O (Eggler and Rosenhauer, 1978), $NaAlSi_3O_8$-H_2O (Eggler and Kadik, 1979; Bohlen et al., 1982; Paillat et al., 1992; Stalder et al., 2000), Mg_2SiO_4-H_2O (Hodges, 1974), and selected peralkaline compositions in the systems K_2O-Al_2O_3-SiO_2-H_2O (Mysen and Acton, 1999), and Na_2O-Al_2O_3-SiO_2-H_2O (Mysen and Wheeler, 2000a).

The melt compositions in many of these experimental studies in the upper mantle temperature/pressure regime are not directly relevant to magmatic processes because their NBO/T (nonbridging oxygen, NBO, per tetrahedrally coordinated cations, T) differs significantly from those of natural magmatic liquids. The NBO/T is a critical factor in the structural control of melt properties (see, for example, Mysen, 1995, for review). The NBO/T range of natural magmatic liquids is between 1 (typical basalt) and near 0 (rhyolite) with andesitic melts intermediate between the two (see Mysen, 1987, for detailed discussion of NBO/T of natural magmatic liquids). The $CaMgSi_2O_6$ and Mg_2SiO_4 melts have NBO/T values of ~2 and ~4, respectively, whereas SiO_2 and $NaAlSi_3O_8$ melts have NBO/T ~0. Melt compositions that fall in the NBO/T range of natural magmatic systems and for which H_2O solubility data are available at upper mantle pressure and temperature conditions, include those in the systems K_2O-Al_2O_3-SiO_2-H_2O (Mysen and Acton, 1999) and Na_2O-Al_2O_3-SiO_2-H_2O (Paillat et al., 1992; Mysen and Wheeler, 2000a; Stalder et al., 2000). Even these data are of limited use, however, because they do not include information on the effect of alkaline earths on the solubility of H_2O in melts. The abundance of alkaline earths in all but the most felsic magmatic liquids exceeds that of alkalis (Chayes, 1975). It is the purpose of the present study, therefore,

* (mysen@gl.ciw.edu).

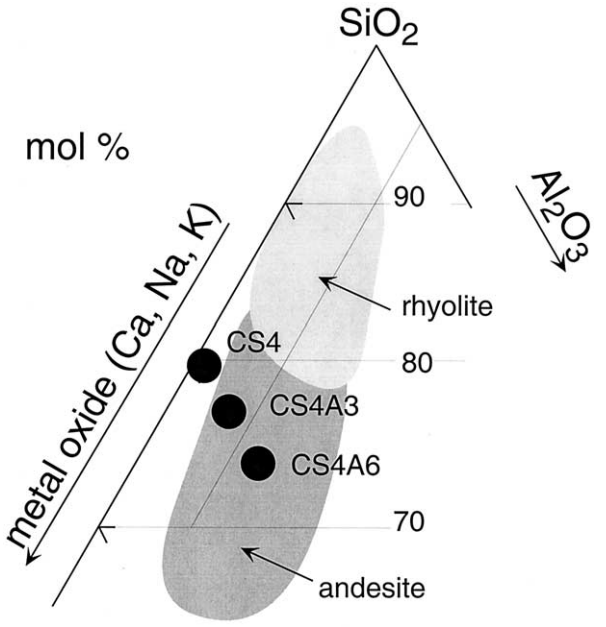

Fig. 1. Composition of starting materials (mol%) in the system metal oxide (Ca, Na, K)-Al_2O_3-SiO_2. The composition fields of rhyolite and andesite are from the database of Chayes (1975).

to provide data on H_2O solubility in peralkaline alkaline earth aluminosilicate melts within the NBO/T range of natural magmatic liquids by determining the solubility of H_2O in melts in the system CaO-Al_2O_3-SiO_2-H_2O. These data can then be compared with H_2O solubility behavior of the Na_2O-Al_2O_3-SiO_2-H_2O and K_2O-Al_2O_3-SiO_2-H_2O melt systems.

2. EXPERIMENTAL METHODS

Starting compositions were along the join $CaSi_4O_9$-$Ca(Ca_{0.5}Al)_4O_9$. Three compositions, CS4 ($CaSi_4O_9$ + 0 mol% Al_2O_3), CS4A3 ($CaSi_4O_9$ + 3 mol% Al_2O_3), and CS4A6 ($CaSi_4O_9$ + 6 mol% Al_2O_3), were used. These compositions were chosen so that on a molar basis, they have Al_2O_3 and SiO_2 concentrations similar to compositions KS4, KS4A3, KS4A6, NS4, NS4A3, and NS4A6 in the systems K_2O-Al_2O_3-SiO_2-H_2O and Na_2O-Al_2O_3-SiO_2-H_2O, for which H_2O solubility data in similar pressure and temperature ranges were reported by Mysen and Acton (1999) and Mysen and Wheeler (2000a). Instead of alkalis, an equivalent proportion of Ca was used (1Ca = 2Na = 2K).[1]

In this manner, we may compare directly the effect of metal cation type on the solubility and solubility behavior of H_2O in these melts. Their compositions are shown together with some major groups of extrusive igneous rocks in Figure 1 (data from Chayes, 1975). The compositions NS4, NS4A3, NS4A6, KS4, KS4A3, and KS4A6 (Mysen and Wheeler, 2000a; Mysen and Acton, 1999) plot at exactly the same positions as CS4, CS4A3, and CS4A6 in this diagram but are not shown.

[1] The compositions KS4, NS4, and CS4 and KS4A3, NS4A3, and CS4A3, and KS4A6, NS4A6, and CS4A6 will be referred to as equivalent compositions throughout the text.

Table 1. Electron microprobe analyses (wt%) of the starting materials[a].

Element	CS4	CS4A3	CS4A6
SiO_2	80.12 ± 0.96[b]	76.69 ± 0.78	75.49 ± 0.88
Al_2O_3	0.28 ± 0.04	4.68 ± 0.08	9.29 ± 0.21
CaO	19.60 ± 0.28	18.63 ± 0.22	15.25 ± 0.15

[a] See text for discussion of sample preparation and analyses.
[b] Standard deviation of average of 10 analytical points.

Starting materials were made from mixtures of $CaCO_3$, Al_2O_3, and SiO_2 ground under alcohol for ~1 h, decarbonated during slow heating (~1.5°C/min), and then heated at 1650°C at 0.1 MPa for 60 min. The samples were then quenched. After this process, starting compositions CS4 and CS4A3 consist of a mixture of a silica polymorph and glass, whereas CS4A6 was a glass.[2] These materials were crushed to ≥20-μm grain size and stored at 110°C when not in use. To obtain a homogeneous glass of these starting materials needed for electron microprobe analysis, a portion of each material was mixed with $LiBO_2$, with $LiBO_2$:silicate = 4:1, melted, and quenched to glass. Electron microprobe analyses of these glasses, obtained with a JEOL model 8900 electron microprobe with 15-kV accelerating voltage and 10-nAmp beam current, and recalculated to 100% silicate, are listed in Table 1. The analyses were conducted while rastering the electron beam across a 10- by 10-μm square to reduce volatilization problems.

High-pressure and high-temperature experiments were conducted in solid-media, high-pressure apparatus (Boyd and England, 1960) with 0.75-inch-diameter furnace assemblies based on the design of Kushiro (1976). Temperatures were measured with Pt-Pt90Rh10 thermocouples with no correction for pressure on their emf. Pressure was calibrated against the melting point of NaCl and the calcite–aragonite transformation. Estimated uncertainties are ±10°C and ±0.1 GPa, respectively.

The silicate starting materials were loaded together with double-distilled, deionized H_2O (1.0 to 2.5 μL depending on desired H_2O content) into 3-mm outer diameter by 7-mm-long Pt containers and welded shut. The weighing accuracy is ±0.02 mg. Water was injected with a microsyringe with 0.1-μL divisions. The exact amount of H_2O added was, however, determined by weighing. Reported H_2O contents of the experimental charges are accurate ±2% or better (2% for the lowest H_2O contents used [~5 wt% of the total sample]). The sealed capsules were kept at 110°C until used in an experiment.

The H_2O solubility in the melts was determined by locating the univariant phase boundary melt ⇔ melt + fluid (Fig. 2 as described by Burnham and Jahns (1962). Mysen and Wheeler (2000a) reproduced the H_2O solubility in $NaAlSiO_3O_8$ melt reported by Burnham and Jahns (1962) to within <2% (relative) with this method. Melts quenched from the field of melt + aqueous fluid (vapor) formed a glass with large vapor bubbles (Fig. 3). These bubbles were clearly visible even in experimen-

[2] Compositions CS4 and CS4A3 are within the field of liquid immiscibility in the system CaO-Al_2O_3-SiO_2 at 0.1 MPa (Osborn and Muan, 1960). Therefore, even at temperatures above the liquidus (>1700°C), two liquids would result.

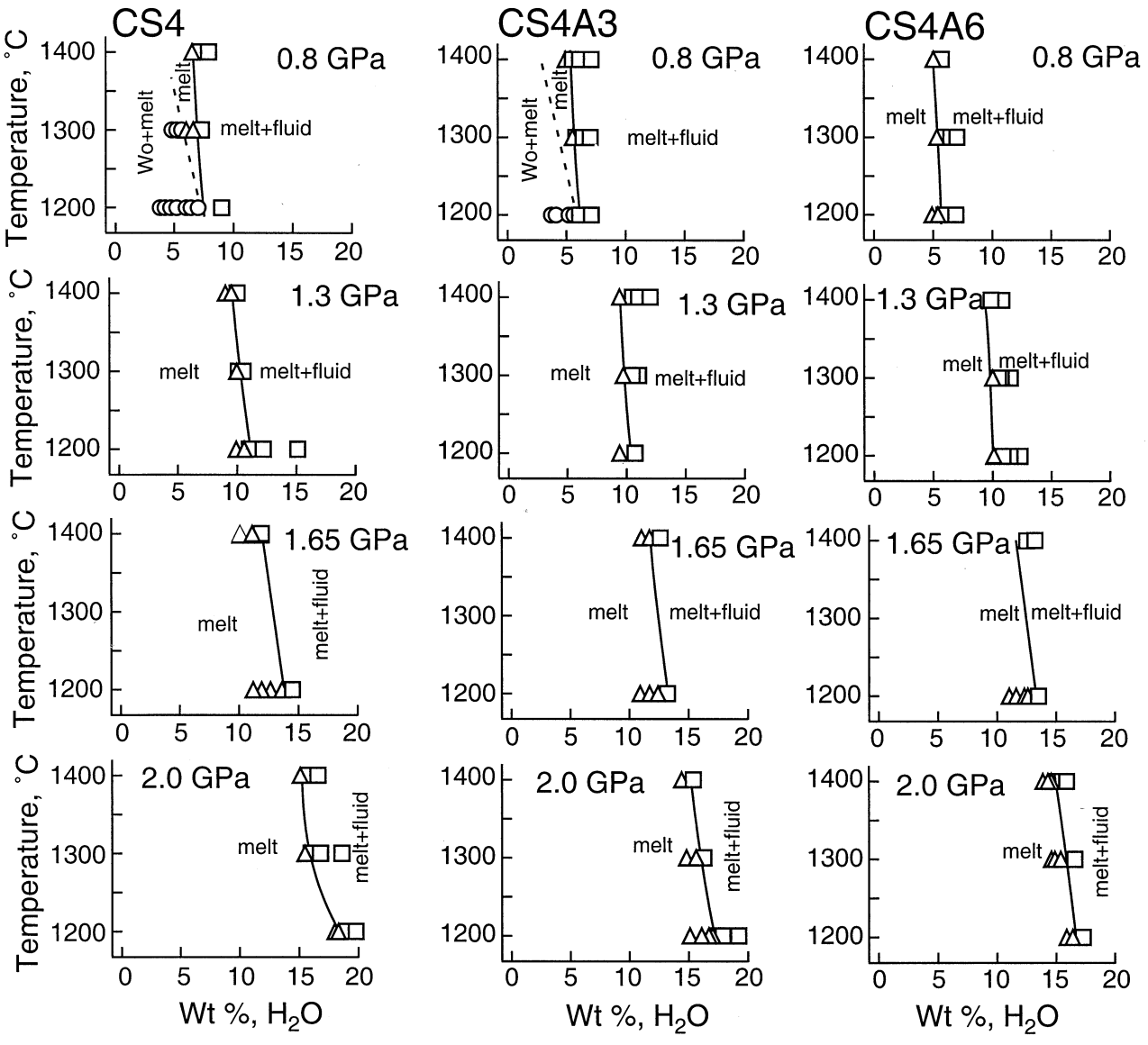

Fig. 2. Experimental results illustrating definition of the melt vs. melt + fluid phase boundary for the compositions and conditions as indicated on individual diagrams.

tal charges where the quenched hydrous melt was nearly completely transformed to a mixture of bubbles and $CaSiO_3$ during quenching (Fig. 3C). Exsolution of H_2O during quenching most likely results from the fact that pressure in the solid-media, high-pressure apparatus decreases during temperature quenching. Because the H_2O solubility decreases with decreasing pressure (Fig. 2), exsolution of H_2O from the melt to form bubbles during this quenching process is difficult to avoid and was a frequent problem during the present experiments. The uncertainty in the H_2O solubility in melts obtained by this method is taken as half that of each of the melt vs. melt + fluid brackets. This uncertainty is generally less than ± 0.5 wt%.

Run durations ranged from 1000 min to 7920 min. Whether these run durations are sufficient to attain equilibrium was evaluated by considering the diffusivity of H_2O in the melts. The diffusion constant, D, for H_2O in silicate melts such as those examined here (haploandesitic in composition) are likely to be somewhere between those of basaltic and rhyolitic melts at the same temperature and with the same H_2O contents. For those melts, the D values range between $\sim 10^{-7}$ and $\sim 10^{-5}$ cm^2/s at temperatures near 1200°C (e.g., Zhang et al., 1991; Nowak and Behrens, 1997). From the simple relationship $x = \sqrt{Dt}$ (x = diffusion distance, D = diffusion constant, and t = time) and with $D = 10^{-7}$ cm^2/s, the diffusion distance of H_2O is ~ 770 μm after 1000 min. With the ≤ 20-μm grain size of the starting material, the 1000- to 7920-min run durations are therefore considered more than adequate to ensure equilibrium during the experiments, provided that melt and aqueous fluid remain well mixed during experimentation. Such mixing is probably accomplished by convection within the 10-mm-long by 3-mm-diameter sample containers owing to the 10°C vertical temperature gradient in the furnaces used (Kushiro, 1976).

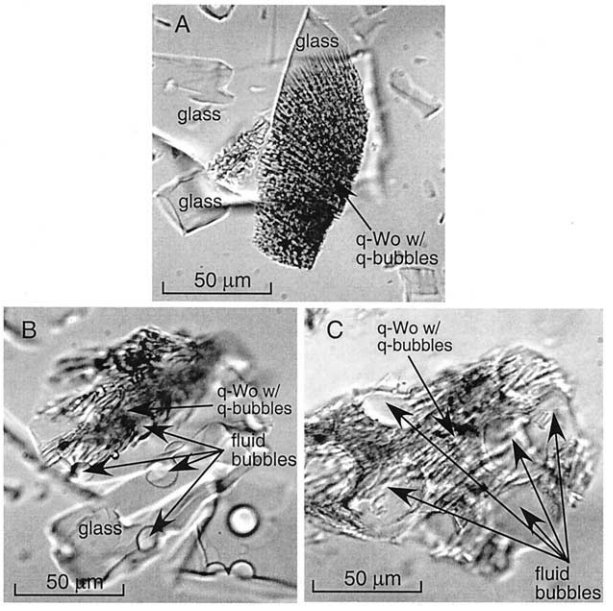

Fig. 3. Photomicrograph of example of quenched glass from within the stability field of melt + aqueous fluid (vapor). Sample CS4 + 15.1 wt% H_2O at 1.3 GPa and 1200°C.

3. RESULTS

The pressure and temperature dependence of the H_2O solubility in the calcium aluminosilicate melts are shown in Figure 4 (solid symbols). For comparison, similar data for the equivalent compositions in the system Na_2O-Al_2O_3-SiO_2-H_2O are also shown (open symbols; data from Mysen and Wheeler, 2000a).

The H_2O solubility, $X^{melt}_{H_2O}$ (mol%, oxygen = 1 in calculation), is a positive and essentially linear function of pressure in this pressure interval at all three temperatures (Fig. 4, Table 2). The pressure dependence, $(\partial X^{melt}_{H_2O}/\partial P)_T$, decreases slightly with increasing temperature and increases with increasing Al_2O_3 content of the melt (Table 2). The $(\partial X^{melt}_{H_2O}/\partial P)_T$ is 25 to 30% smaller than that observed for the equivalent compositions in the Na_2O-Al_2O_3-SiO_2-H_2O system (Mysen and Wheeler, 2000a; see also open symbols in Figure 4 and 15 to 40% smaller than for equivalent melt compositions in the K_2O-Al_2O_3-SiO_2-H_2O (Mysen and Acton, 1999).

The H_2O solubility in Ca-aluminosilicate melts decreases with increasing temperature at all pressures (Fig. 4, Table 2) with a temperature dependence, $(\partial X^{melt}_{H_2O}/\partial T)_P$, on the order of 1 mol% H_2O/100°C. Again, this behavior resembles that observed for melts in the peralkaline portions of the alkali aluminosilicate systems Na_2O-Al_2O_3-SiO_2-H_2O (Mysen and Wheeler, 2000a; see also open symbols in Figure 4 and K_2O-Al_2O_3-SiO_2-H_2O (Mysen and Acton, 1999). The temperature dependence of the H_2O solubility in the equivalent alkali aluminosilicate melts is, however, greater by as much as 40% compared with the $(\partial X^{melt}_{H_2O}/\partial T)_P$ for equivalent melts in the CaO-Al_2O_3-SiO_2-H_2O system.

Increasing Al_2O_3 results in lower H_2O solubility at constant pressure and temperature (Fig. 5), similar to other aluminosilicate melts (e.g., Dingwell et al., 1997). The effect of Al_2O_3 appears significantly less pronounced for melts along the join $CaSi_4O_9$-$Ca(Ca_{0.5}Al)_4O_9$ than for those along the $Na_2Si_4O_9$-$Na_2(NaAl)_4O_9$ join (Mysen and Wheeler, 2000a; see also open symbols in Fig. 5).

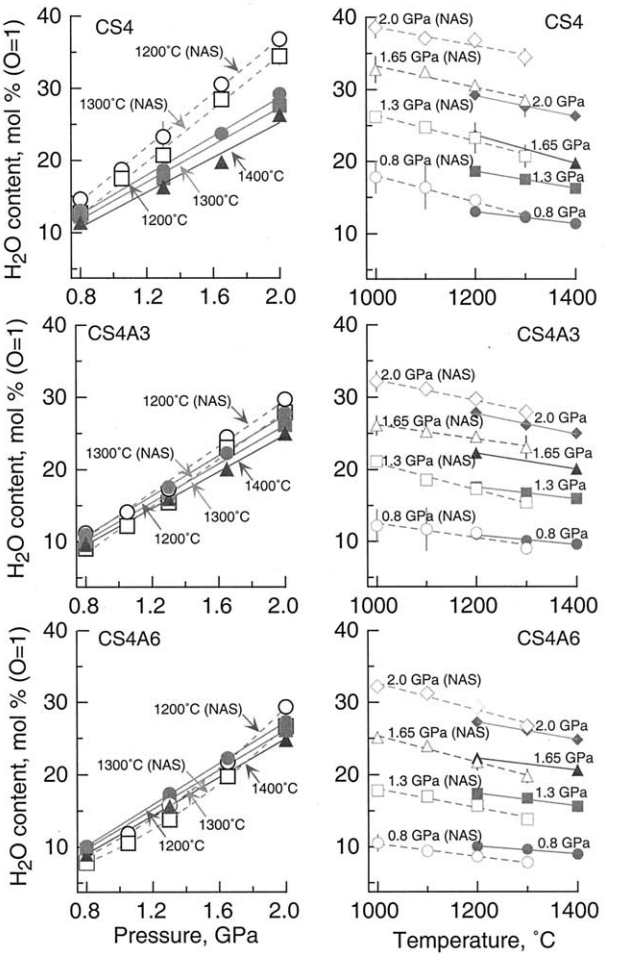

Fig. 4. Pressure and temperature dependence of H_2O solubility in CS4, CS4A3, and CS4A6 composition melts (solid symbols). Also shown (open symbols) are the H_2O solubilities in the equivalent NS4, NS4A3, and NS4A6 composition melts (data from Mysen and Wheeler, 2000a). When error bars are not shown, errors are smaller than symbol size.

The pressure, temperature, and composition dependence of H_2O solubility in CaO-Al_2O_3-SiO_2-H_2O melts can be combined via stepwise regression to obtain the relationship

$$X^{melt}_{H_2O}(CAS) = 18.6 \pm 1.6 - 0.67 \pm 0.13 \cdot X_{Al} + 0.063 \pm 0.02 \cdot (X_{Al})^2 + 13.3 \pm 0.2 \cdot P - 0.011 \pm 0.001 \cdot T. \quad (1)$$

Here, $X^{melt}_{H_2O}$ (CAS) and X_{Al} are in mol%, T is temperature (K), and P is pressure (GPa). The expression for the equivalent melt compositions in the Na_2O-Al_2O_3-SiO_2-H_2O system (Mysen and Wheeler, 2000a) is

$$X^{melt}_{H_2O}(NAS) = 22.3 \pm 1.4 - 2.4 \pm 0.2 \cdot X_{Al} + 0.21 \pm 0.2 \cdot (X_{Al})^2 + 17.3 \pm 0.2 \cdot P + 0.0144 \pm 0.0009 \cdot T. \quad (2)$$

Here, the larger coefficients reflect the more significant pres-

Table 2. Temperature $(\partial X^{melt}_{H_2O}/\partial T)_P$, and pressure dependence, $(\partial X^{melt}_{H_2O}/\partial P)_T$, of H_2O solubility in CaO-Al_2O_3-SiO_2-H_2O melts.

Variable	CS4	CS4A3	CS4A6
		$(\partial X^{melt}_{H_2O}/\partial P)_T$ (mol%/GPa)	
T (°C)			
1200	13.49 (0.81)[a]	13.99 (0.44)	14.32 (0.3)
1300[b]	12.94 (1.06)	13.38 (0.05)	13.71 (0.21)
1400	12.09 (1.49)	12.75 (0.28)	13.32 (0.28)
		$(\partial X^{melt}_{H_2O}/\partial T)_P \cdot 10^3$ (mol%/°C)	
Pressure (GPa)			
0.8	−0.0084 (0.0002)	−0.0067 (0.0010)	−0.0055 (0.0007)
1.3	−0.0117 (0.0005)	−0.0083 (0.0002)	−0.0087 (0.0014)
1.65[b]	−0.0199	−0.011	−0.0083
2.0	−0.0144 (0.0010)	−0.014 (0.02)	−0.0122 (0.0005)

[a] $\pm 1\sigma$ error from linear regression.
[b] Three data points, no error calculation.

sure, temperature, and composition dependence of the H_2O solubility in melts in the Na_2O-Al_2O_3-SiO_2H_2O system.

4. DISCUSSION

4.1. Melt Composition and H_2O Solubility

There are two distinct differences in H_2O solubility in Ca- and alkali (Na and K)–silicate melts. First, for compositions with the same Al_2O_3 content, the H_2O solubility in alkali-silicate melts is higher and significantly more dependent on pressure and temperature than Ca-silicate melts (Fig. 4). Second, the H_2O solubility in alkali-silicate melts is more sensitive to Al_2O_3 than Ca-silicate melts (Fig. 5).

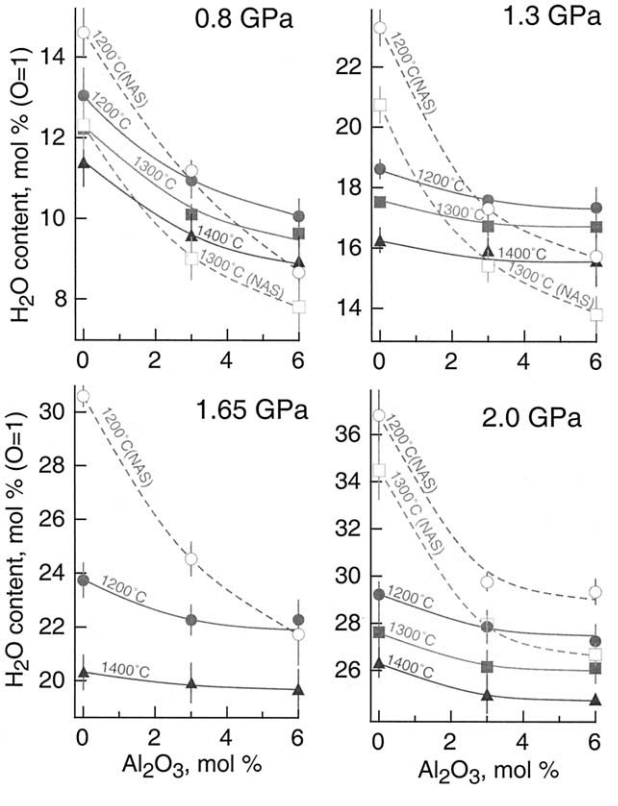

Fig. 5. Effect of bulk Al_2O_3 content on the H_2O solubility at temperatures and pressures shown. Closed symbols = melts in the system CaO-Al_2O_3-SiO_2; open symbols = melts in the system Na_2O-Al_2O_3-SiO_2 (data from Mysen and Wheeler, 2000a). When error bars are not shown, errors are smaller than symbol size.

There are structural differences between alkali- and Ca-silicate melts that may help explain why these differences exist. In both alkali- and Ca-silicate melts such as those considered here, equilibrium between the structural units in these melts can be described as

$$2Q^3 \Leftrightarrow Q^2 + Q^4. \quad (3)$$

The ΔH for this reaction is positively correlated with the ionization potential of metal cations in alkali and alkaline earth–silicate melts (Mysen, 1995). Therefore, the concentration and activity of Q^2 and Q^4 species in Ca-silicate melts is considerably greater than in alkali-silicate melts. As a result, structural interaction between H_2O (to form OH complexes) and the silicate species in the melts will be affected by the ionization potential of the metal cation. Further, structural data from the systems Na_2O-SiO_2-H_2O and CaO-SiO_2-H_2O indicate that in addition to Si..OH, in the alkali system, Na..OH complexes are formed, whereas in the Ca system, Ca..OH complexes are formed (Mysen and Virgo, 1986a,b). Although none of these effects currently can be placed on a quantitative footing, these structural differences may well account for the different solubility behavior of H_2O in Ca and alkali-silicate melts.

The different effects of Al_2O_3 on H_2O solubility may also relate to the different electronic properties of the metal cations. In Al-bearing Ca-silicate melts, Ca^{2+} serves to charge-balance Al^{3+} in tetrahedral coordination (formally, 1 Ca^{2+} will charge balance 2 Al^{3+} in tetrahedral coordination), whereas in the alkali systems, K^+ or Na^+ serves this purpose (1 alkali/1 Al^{3+} in tetrahedral coordination). These differences results in different thermodynamic properties of Ca- vs. alkali-silicate melts (e.g., Merzbacher and White, 1991; Richet and Neuville, 1992; Toplis, 1998; Romano et al., 2001). Although we do not know how these differences translate to H_2O solubility, it is suggested that the different electronic properties of Al^{-3+} charge-balanced with Ca^{2+} compared with alkalis will also affect the

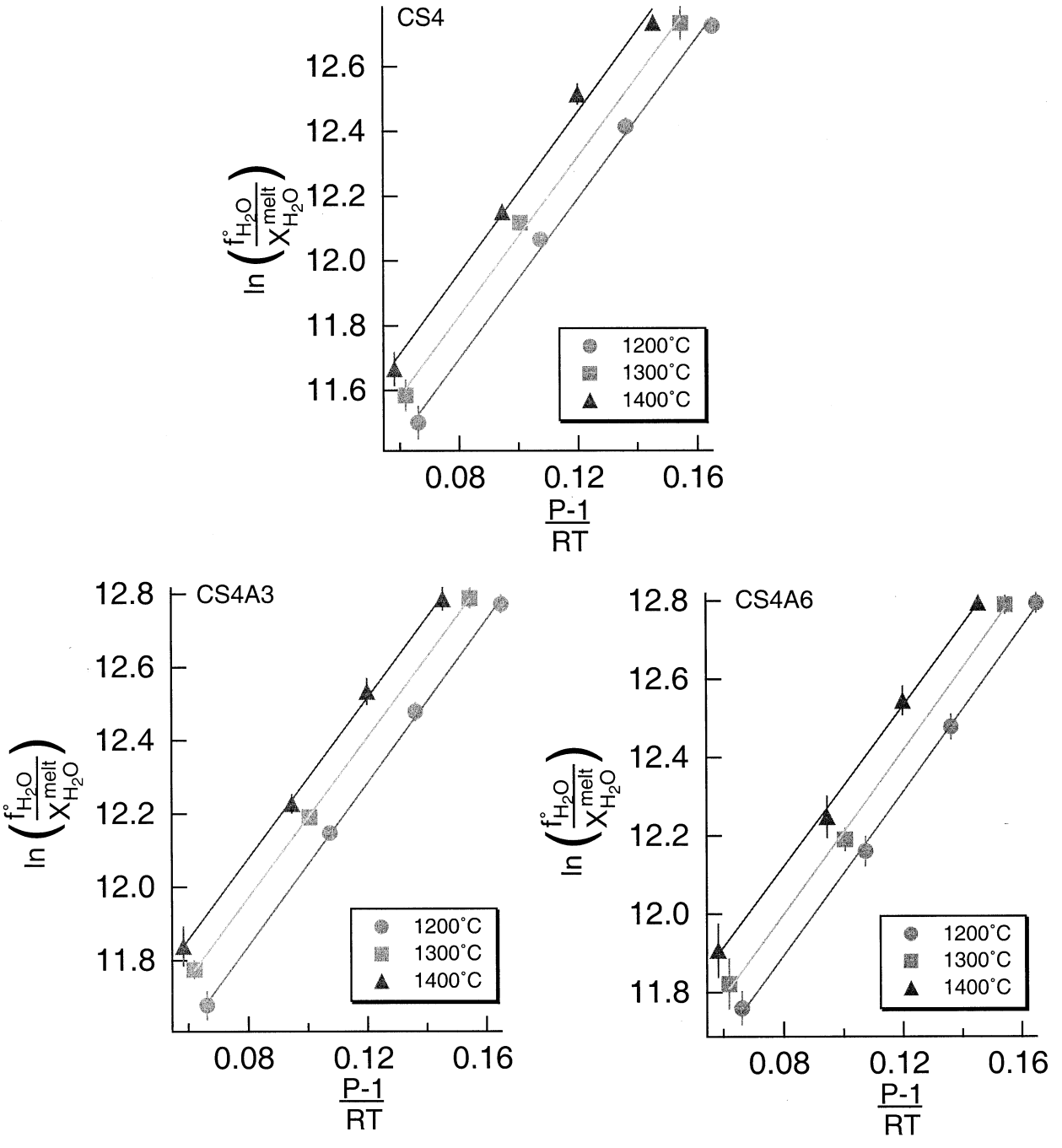

Fig. 6. Relationship between $\ln(f^{\circ}_{H_2O}/X^{melt}_{H_2O})$ and $(P-1)/RT$ at temperatures indicated on figures for compositions CS4, CS4A3, and CS4A6. When error bars are not shown, errors are smaller than symbol size. Regression coefficients are listed in Table 3. See text for more detailed discussion.

relationship between H_2O solubility and Al_2O_3 content of the melts.

4.2. Partial Molar Volume of H_2O in Melts

The H_2O solubility data in CaO-Al_2O_3-SiO_2 melts have been used to calculate partial molar volumes of H_2O in the melts. For H_2O-saturated silicate melt in equilibrium with free H_2O, the Gibbs free energy of solution of H_2O is (J/mol) (Hodges, 1974);

$$\Delta G_T(P) = 0 = \Delta G_T\,(1bar) + RT \ln \frac{a^{melt}_{H_2O}}{f^{o}_{H_2O}} + \int_1^P \bar{V}^{melt}_{H_2O}\, dP, \qquad (4)$$

Table 3. Regression coefficients for linear fit to, $\ln(f_{H_2O}/X^{melt}_{H_2O}) = a + b[(P - 1)/RT]$.

	CS4		CS4A3		CS4A6	
T (°C)	a	b	a	b	a	b
1200	10.71 ± 0.06	12.4 ± 0.5	10.95 ± 0.03	11.2 ± 0.2	11.06 ± 0.03	10.5 ± 0.2
1300	10.84 ± 0.08	12.3 ± 0.7	10.10 ± 0.01	11.0 ± 0.1	11.16 ± 0.05	10.5 ± 0.4
1400	10.96 ± 0.09	12.5 ± 0.8	11.20 ± 0.03	11.0 ± 0.2	11.30 ± 0.03	10.3 ± 0.3

where R is the universal gas constant (82.157 cm^3bar/mol K), T is temperature (K), $a^{melt}_{H_2O}$ is activity of H_2O in the melt, $f^{o}_{H_2O}$ is the fugacity of pure H_2O in bar (data of Haar et al., 1984, are used here), and $\bar{V}^{melt}_{H_2O}$ (cm^3/mol) is the partial molar volume of H_2O in the melt. In Eqn. 4, possible effects on f_{H_2O} of silicate dissolved in the coexisting aqueous fluid is ignored. The silicate solubility in these aqueous fluids is, however, ≤4 mol%, depending on silicate composition, pressure, and temperature in the composition, pressure, and temperature range considered here (Mysen, 2002). Unless there are large deviations from ideal mixing in these silicate-bearing aqueous fluids, such small amounts of dissolved silicate would not affect $\bar{V}^{melt}_{H_2O}$ within the experimental uncertainty.

The activity of H_2O, $\bar{V}^{melt}_{H_2O}$, is not known. Provided that the activity coefficient of H_2O in the melt, $\gamma^{melt}_{H_2O}$, does not vary over the pressure, temperature, and H_2O concentration range considered here, the mol fraction of H_2O, $X^{melt}_{H_2O}$, may be substituted for $a^{melt}_{H_2O}$.

The slope of the $(P - 1)/RT$ vs. $\ln(f^{o}_{H_2O}/X^{melt}_{H_2O})$ equals $\bar{V}^{melt}_{H_2O}$ at temperature T, provided that $\gamma^{melt}_{H_2O}$ remains constant (Fig. 6; see Table 3 for regression coefficients). In the 0.8- to 2.0-GPa pressure range under isothermal conditions, these lines are straight (Fig. 6) and consistent with the assumption that $\gamma^{melt}_{H_2O}$ is constant. Straight lines could also be obtained if there was a pressure dependence of $\bar{V}^{melt}_{H_2O}$ and that such a pressure dependence was canceled out by the pressure dependence of $\gamma^{melt}_{H_2O}$. Such a situation is, however, considered highly unlikely. The straight lines in Figure 6 most likely imply that the partial molar volume of H_2O in the melts, $\bar{V}^{melt}_{H_2O}$, does not vary with pressure in 0.8 to 2.0 GPa pressure range within the uncertainty of the calculated partial molar volume values (Figs. 6 and 7). The uncertainty in $\bar{V}^{melt}_{H_2O}$ reflects the progression of the errors in the measured H_2O solubilities for the melts.

The $\bar{V}^{melt}_{H_2O}$ in the CaO-Al_2O_3-SiO_2-H_2O system ranges between 10.4 and 12.4 cm^3/mol and decreases with increasing Al_2O_3 (Fig. 7). This behavior is qualitatively similar to the behavior of $\bar{V}^{melt}_{H_2O}$ in Na_2O-Al_2O_3-SiO_2-H_2O and K_2O-Al_2O_3-SiO_2-H_2O melts. The partial molar volume of H_2O in CaO-Al_2O_3-SiO_2-H_2O melts is insensitive to temperature (Fig. 7, Table 4) in contrast to Na_2O-Al_2O_3-SiO_2-H_2O and K_2O-Al_2O_3-SiO_2-H_2O melts, where $\bar{V}^{melt}_{H_2O}$ decreases with increasing temperature (Fig. 7).

The partial molar volume of H_2O in the alkali and alkaline earth aluminosilicate melts depends on the type of metal cation. The $\bar{V}^{melt}_{H_2O}$ (CAS)[3] is ~10% higher than $\bar{V}^{melt}_{H_2O}$ (NAS), and $\bar{V}^{melt}_{H_2O}$ (NAS) is 6 to 8% higher than $\bar{V}^{melt}_{H_2O}$ (KAS) at 1200°C for the same bulk Al_2O_3 content. The difference between $\bar{V}^{melt}_{H_2O}$ in alkaline earth and alkali aluminosilicate melts increases with increasing temperature. The $\bar{V}^{melt}_{H_2O}$ differences most probably result from differences in solution mechanisms of H_2O in the melts as discussed above.

The $\bar{V}^{melt}_{H_2O}$ values in Figure 7 compare reasonably well with those calculated from water solubility data for haplogranite ($Qz_{28}Ab_{38}Or_{34}$), albite, and diopside composition melts (Burnham and Davis, 1971; Hodges, 1974; Paillat et al., 1992; Holtz et al., 1995), for a composition in the CaO-Al_2O_3-SiO_2-H_2O system by McMillan et al. (1986) [NBO/T = 0.6, Al/(Al + Si) + 0.14], and for andesite glass (Richet and Polian, 1998). The H_2O solubility data of McMillan et al. (1986) at 1180°C for a CaO-Al_2O_3-SiO_2 melt, when extrapolated to 0.8 GPa, yields a $\bar{V}^{melt}_{H_2O}$ value of 9.5 cm^3/mol. The latter composition resembles CS4A6, for which $\bar{V}^{melt}_{H_2O}$ = 10.4 cm^3/mol at 0.8 GPa and 1200°C. The H_2O solubility data of Holtz et al. (1995) for $Qz_{28}Ab_{38}Or_{34}$ melt between 0.03 and 0.8 GPa at 800°C, yields values for $\bar{V}^{melt}_{H_2O}$ that appear to decrease exponentially from ~32 cm^3/mol at 0.03 GPa to ~12.5 cm^3/mol at 0.5 GPa. The 1400°C H_2O solubility isotherm for $NaAlSi_3O_8$ melt (Paillat et al., 1992) results in the apparent $\bar{V}^{melt}_{H_2O}$ decreasing as a nonlinear function of pressure from ~ 41 to ~ 12 cm^3/mol between 0.2 and 0.4 GPa. The $\bar{V}^{melt}_{H_2O}$ data in Figure 7, as well as those derived from literature solubility data, are somewhat lower than those deduced from thermal expansion and compressibility data of $NaAlSi_3O_8$-H_2O glass and melt by Ochs and Lange (1997) (17 to 20 cm^3/mol).

The composition and temperature dependence of the partial molar volume of H_2O in silicate melts (Fig. 7) may be used to estimate the partial molar volume of H_2O in melts of natural compositions. In this calculation it is assumed that the $\bar{V}^{melt}_{H_2O}$ in the compositionally more complex natural melts is an additive function of $\bar{V}^{melt}_{H_2O}$ determined for each of the simple ternary aluminosilicate melt compositions. Before summing up the $\bar{V}^{melt}_{H_2O}$ values, the effect of Al_2O_3 on $\bar{V}^{melt}_{H_2O}$ was estimated by extrapolating the relationship between $\bar{V}^{melt}_{H_2O}$ and Al_2O_3 for the individual cations (Na, K, and Ca) (Fig. 7) to the Al/(Al + Si) of the natural melt compositions (Table 5). In the absence of $\bar{V}^{melt}_{H_2O}$ data on Mg- and Fe-bearing systems, it was assumed that the contribution from the alkaline earths and ferrous iron could be modeled with the CaO-Al_2O_3-SiO_2-H_2O melt data obtained here (Fig. 7).

Three examples of $\bar{V}^{melt}_{H_2O}$ calculated for natural magmatic liquids, which use average compositions of dacite, andesite, and tholeiite (Table 5), are shown in Figure 8. The $\bar{V}^{melt}_{H_2O}$ decreases in the order $\bar{V}^{melt}_{H_2O}$ (tholeiite melt) > $\bar{V}^{melt}_{H_2O}$ (andesite melt > $\bar{V}^{melt}_{H_2O}$ (dacite melt) at the same temperature. For the temperature dependence, we find that $(\partial X^{melt}_{H_2O}/\partial T)_P$ (dacite melt) > $(\partial X^{melt}_{H_2O}/\partial T)_P$ (andesite melt) > $(\partial X^{melt}_{H_2O}/\partial T)_P$ (tholeiite melt).

[3] CAS, CaO-Al_2O_3-SiO_2-H_2O; NAS, Na_2O-Al_2O_3-SiO_2-H_2O; and KAS, K_2O-Al_2O_3-SiO_2-H_2O.

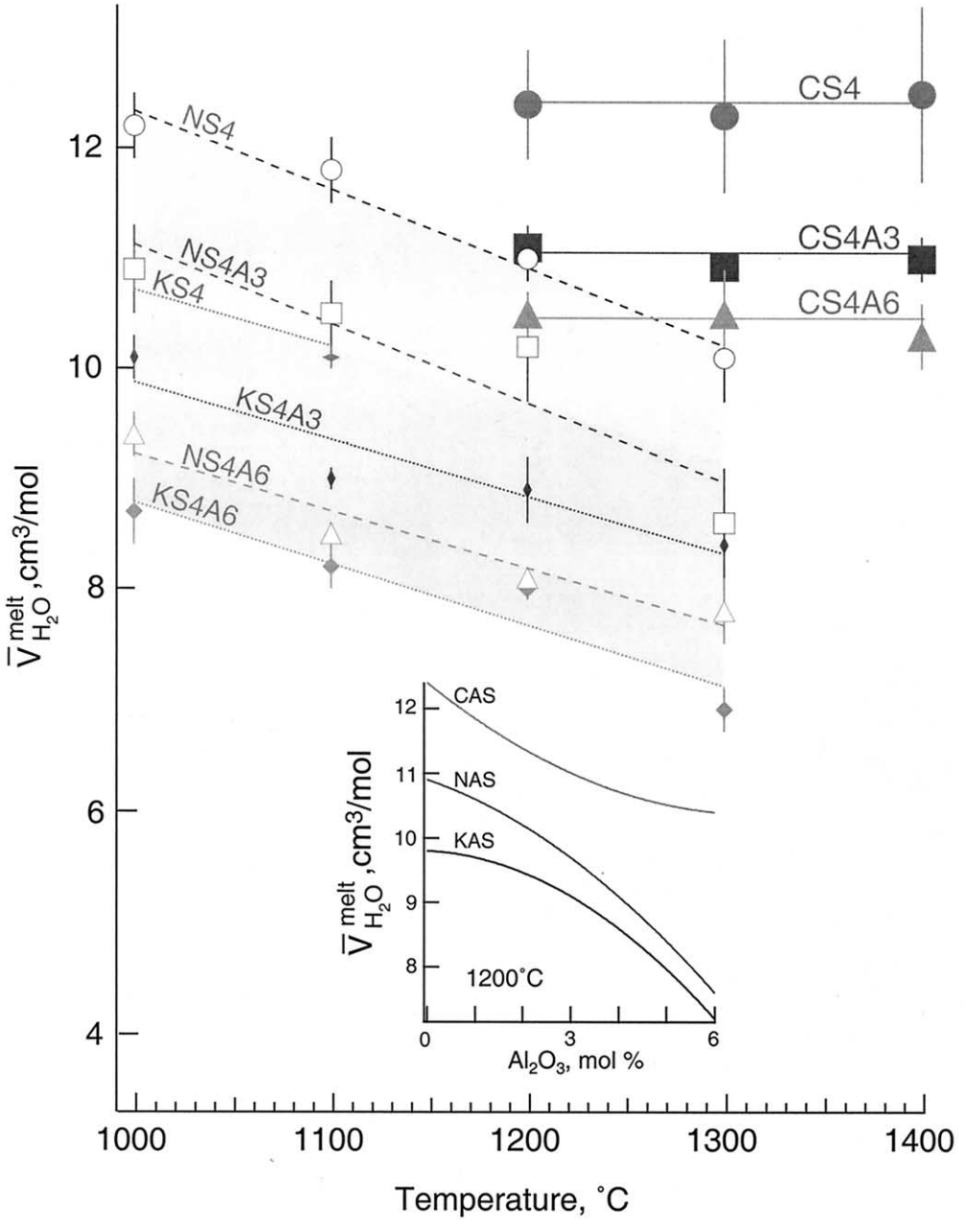

Fig. 7. Partial molar volume of H_2O in aluminosilicate melts, $\bar{V}^{melt}_{H_2O}$, as a function of temperature for compositions shown. The data for alkali aluminosilicate melts are from Mysen and Acton (1999) and Mysen and Wheeler (2000a). Insert: $\bar{V}^{melt}_{H_2O}$ as a function of Al_2O_3 at 1200°C for melts in the system CaO-Al_2O_3-SiO_2 (CAS), Na_2O-Al_2O_3-SiO_2 (NAS), and K_2O-Al_2O_3-SiO_2.

The relationship between $\bar{V}^{melt}_{H_2O}$ values and melt type follows from the relative abundance of alkali metals (and proportion of K and Na) and alkaline earths in the three natural melt compositions (Table 5). Dacite has the greatest proportion of alkali metals (and the greater fraction of potassium) followed by andesite and finally tholeiite. As $\bar{V}^{melt}_{H_2O}$ (KAS) < $\bar{V}^{melt}_{H_2O}$ (NAS) < $\bar{V}^{melt}_{H_2O}$ (CAS) (Fig. 7), the relative values of $\bar{V}^{melt}_{H_2O}$ for the natural melts shown in Figure 8 follows. Furthermore, $(\partial X^{melt}_{H_2O}/\partial T)_P$ for alkali aluminosilicate melts exceeds $(\partial X^{melt}_{H_2O}/\partial T)_P$ of alkaline earth aluminosilicate melts (Table 4).

4.3. Density of Hydrous and Anhydrous Melts

The density of anhydrous and water-saturated CS4, CS4A3 and CS4A6 melts was calculated with the $\bar{V}^{melt}_{H_2O}$ and H_2O solubility data from the present study coupled with thermal expansion and compressibility data of anhydrous oxide components (Lange and Carmichael, 1987; Kress and Carmichael, 1991). In these calculations, it is assumed that the partial molar volume of these oxide components obtained for anhydrous melts is the same in hydrous melts. In light of the lack of

Table 4. Regression coefficients for liner fit to the function, $\bar{V}^{melt}_{H_2O}$ = a + bT(°C).

Composition	a	b
CS4	12.4 ± 0.2	—
CS4A3	11.01 ± 0.07	—
CS4A6	10.4 ± 0.1	—
NS4[a]	19.4 ± 0.8	−0.0071 ± 0.0008
NS4A3[a]	18.3 ± 2.5	−0.0071 ± 0.002
NS4A6[a]	14.8 ± 1.9	−0.006 ± 0.002
KS4[b]	15.9 ± 0.7	−0.0051 ± 0.0007
KS4A3[b]	15.1 ± 1.6	−0.055 ± 0.001
KS4A6[b]	14.4 ± 1.5	−0.006 ± 0.001

[a] From solubility data of Mysen and Wheeler (2000a).
[b] From solubility data of Mysen and Acton (1999).

composition dependence of those partial molar volume values in anhydrous melts, this assumption seems reasonable. The density difference between anhydrous and hydrous Ca-aluminosilicate melts (thick lines) are compared with the density difference between anhydrous and hydrous melts for the equivalent compositions in the Na_2O-Al_2O_3-SiO_2-H_2O system (Fig. 9). For H_2O-saturated melts, the density difference for Na-aluminosilicate melts is ~5% less than that for Ca-aluminosilicate melts. This difference in the melt density is in part because the partial molar volume of H_2O in the Ca-aluminosilicate melts is ~10% higher than in the equivalent Na-aluminosilicate melts (Fig. 7), and in part because the solubility of H_2O in the Na-aluminosilicate melts is slightly greater than in the Ca-bearing melts (Fig. 4). The partial molar volumes of CaO and Na_2O are also slightly different (Lange and Carmichael, 1987; Kress and Carmichael, 1991), thus further contributing to the difference in density between the two systems.

The density of H_2O-saturated, Al-free CS4 ($CaSi_2O_9$) melt is nearly 27% less than that of an anhydrous CS4 melt at 2.0 GPa. This density difference diminishes with increasing Al_2O_3 content and reaches ~22% for the most aluminous composition, CS4A6, at 2.0 GPa. The dominating influence of H_2O on the melt density is the partial molar volume of H_2O and H_2O solubility in the melt, both of which decrease with increasing Al_2O_3 (Figs. 5 and 7). As a result, the more aluminous the melt, the less of a density difference between anhydrous and H_2O-saturated melts whether in alkaline earth or alkali aluminosilicate systems (Fig. 9A). The density difference between H_2O-saturated and anhydrous melts decreases with decreasing pressure (Fig. 9A) because the H_2O solubility of the melts decreases with decreasing pressure (Fig. 4).

Table 5. Average composition (wt%) of common extrusive igneous rocks[a].

Element	Dacite (338)[b]	Andesite (2068)[b]	Tholeiite (1010)[b]
SiO_2	65.23	57.71	48.62
TiO_2	0.62	0.88	2.00
Al_2O_3	15.79	17.25	15.1
FeO	4.78	7.81	10.81
MnO	0.11	0.14	0.17
MgO	1.75	3.42	7.84
CaO	4.62	7.09	10.17
Na_2O	3.76	3.36	2.76
K_2O	2.08	1.57	0.84
Al/(Al + Si)	0.22	0.26	0.27
K+/(alkali + alkaline earth)	0.15	0.09	0.04
Na+/(alkali + alkaline earth)	0.42	0.31	0.18
Alkaline earth/(alkali + alkaline earth)	0.43	0.60	0.78

[a] Alkaline = total alkalis (Na + K) (molar proportion); Alkaline earth: total alkaline earths (Ca + Mg) (molar proportion).
[b] Average analyses obtained from the data base of Chayes (1975) for Cenozoic extrusive igneous rocks. The number in parentheses denotes the number of analyses in the average.

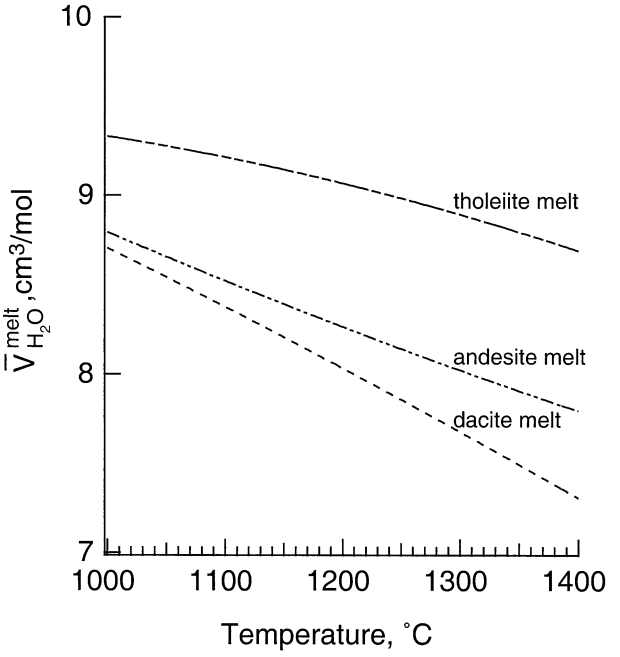

Fig. 8. Partial molar volume of H_2O, $\bar{V}^{melt}_{H_2O}$, calculated for dacite, andesite, and tholeiite melt (Table 5) as a function of temperature. The functions describing the temperature dependence are: $\bar{V}^{melt}_{H_2O}$ (dacite) = 11.2 to 0.0018T − 7.1 × $10^{-7}T^2$ (°C), $\bar{V}^{melt}_{H_2O}$ (andesite) = 12.3-0.0042T − 7.1 × $10^{-7}T^2$, and $\bar{V}^{melt}_{H_2O}$ (tholeiite) = 8.9 + 0.0018T-1.4 × $10^{-6}T^2$.

For melts with constant H_2O content less than the saturation value, the pressure effect on the density difference is smaller (Figs. 9B–D). In comparison with Na-aluminosilicate melts, there is a greater density difference between anhydrous and hydrous Ca-aluminosilicate melts for all H_2O contents. The slight positive correlation of the density difference with pressure even with H_2O-undersaturated melts (Fig. 9B–D) results from the use of a constant partial molar volume of H_2O in the range 0.8 to 2.0 GPa, whereas the pressure derivatives of the oxide volumes are slightly negative (Kress and Carmichael, 1991). The inverse correlation between density difference and Al_2O_3 content for H_2O-saturated melts (Fig. 9A) remains with constant H_2O content (Fig. 9B–D) because of the negative correlation between $\bar{V}^{melt}_{H_2O}$ and Al_2O_3 of the melt.

The effect of dissolved H_2O on the density of dacite, andesite, and tholeiite melt (Fig. 10) was determined from the partial molar volume of H_2O (Fig. 8) combined with the partial molar volumes of oxides (Lange and Carmichael, 1987; Kress and Carmichael, 1991). The influence of H_2O content on the density of tholeiite melt is more pronounced than for andesite. The

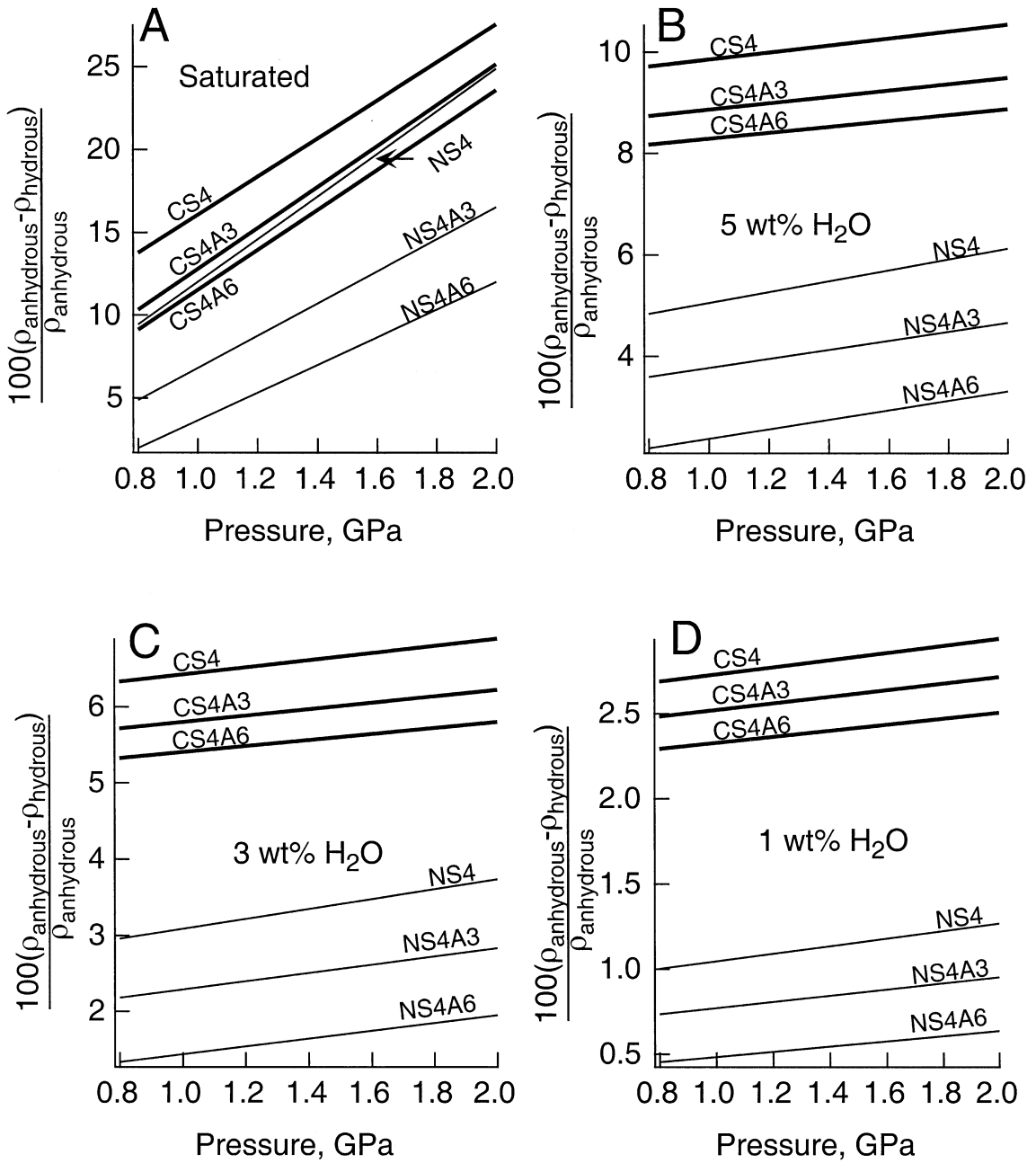

Fig. 9. Density difference between anhydrous and H_2O-bearing CS4, CS4A3, and CS4A6 melts as a function of pressure. Also shown are data from Mysen and Wheeler (2000a) for the equivalent compositions NS4, NS4A3, and NS4A6 in the system Na_2O-Al_2O_3-SiO_2-H_2O. (A) H_2O-saturated melts. (B) Melts with 5 wt% H_2O. (C) Melts with 3 wt% H_2O. (D) Melts with 1 wt% H_2O.

effect on andesite melt is greater than for dacite melt regardless of H_2O content chosen (Fig. 10). The density difference between anhydrous tholeiite melt and tholeiite melt with 3 wt% in solution is approximately the same as the effect of 5 wt% H_2O dissolved in dacite melt. These differences result from the larger fraction of alkaline earths in the tholeiite compared with andesite and in andesite compared with dacite melt. The density differences between hydrous and anhydrous Ca-aluminosilicate melts is considerable greater than for equivalent Na- and K-aluminosilicate melts (Fig. 9).

4.4. Extrapolation of $\bar{V}^{melt}_{H_2O}$ to Crustal Pressure Conditions

The $\bar{V}^{melt}_{H_2O}$ data obtained at high pressure (0.8 to 2.0 GPa) may be applied to crustal magmatic processes involving H_2O-rich

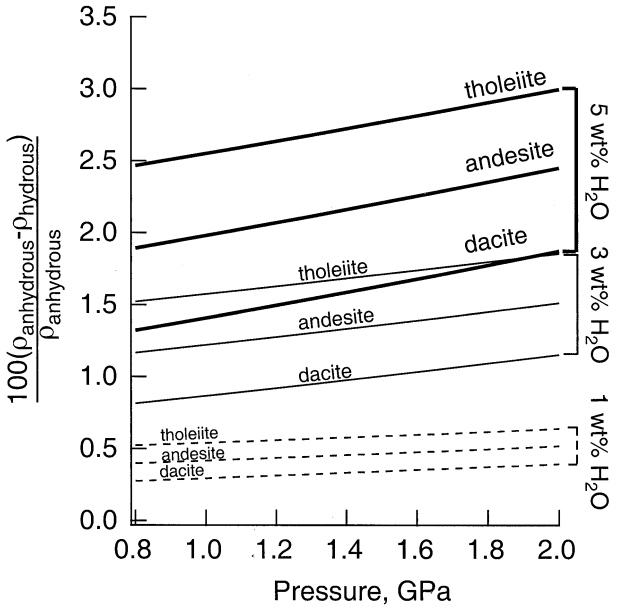

Fig. 10. Density difference between anhydrous and H_2O-bearing dacite, andesite, and tholeiite melts as a function of pressure for 5 wt% H_2O (thick lines), 3 wt% H_2O (thin lines), and 1 wt% H_2O (dashed lines).

magma provided that the high-pressure $\bar{V}_{H_2O}^{melt}$ data can be extrapolated to lower pressures. The straight-line fits in Fig. 6 are consistent with a suggestion that at least in the 0.8- to 2.0-GPa pressure range, $\bar{V}_{H_2O}^{melt}$ is not sensitive to pressure or to the H_2O content of the melts at H_2O saturation values in this pressure range (Fig. 4). These results are similar to those of the K_2O-Al_2O_3-SiO_2 and Na_2O-Al_2O_3-SiO_2 systems in the same pressure and temperature range (Mysen and Acton, 1999; Mysen and Wheeler, 2000a).

If, however, we consider published H_2O solubility data at lower pressures (<0.8 GPa) for compositions such as $NaAlSi_3O_8$ (Paillat et al., 1992) and the haplogranite melt composition, $Qz_{28}Ab_{38}Or_{34}$ (Holtz et al., 1995), the $\bar{V}_{H_2O}^{melt}$ calculated from the H_2O solubility, again assuming $\gamma_{H_2O}^{melt}$ = constant, exhibits a pronounced increase in $\bar{V}_{H_2O}^{melt}$ as the pressure is decreased (Mysen and Wheeler, 2000a). For example, at 1200°C, the $\bar{V}_{H_2O}^{melt}$ calculated in this manner from the H_2O solubility in $Qz_{28}Ab_{38}Or_{34}$ composition melt at 1200°C (Holtz et al., 1995) increases from 12.5 cm^3/mol at 0.5 GPa to ~40 cm^3/mol at 0.1 GPa (Mysen and Wheeler, 2000a). An even more pronounced apparent pressure dependence of $\bar{V}_{H_2O}^{melt}$ is obtained from the H_2O solubility in the CaO-Al_2O_3-SiO_2 melts to ≤0.5 GPa at 1180°C from McMillan et al. (1986). Those latter $\bar{V}_{H_2O}^{melt}$ values are compared with those of CS4A6 melt,[4] calculated from Fig. 6, in Fig. 11A. The apparent $\bar{V}_{H_2O}^{melt}$ decreases from ≥120 cm^3/mol at 0.01 GPa to ~22 cm^3/mol at 0.5 GPa at ~1200°C (Fig. 11A, B). Those $\bar{V}_{H_2O}^{melt}$ values can be extrapolated smoothly to the $\bar{V}_{H_2O}^{melt}$ values for CS4A6 at P ≥ 0.8 GPa, where there is no apparent pressure dependence of $\bar{V}_{H_2O}^{melt}$ with a further pressure increase ($\bar{V}_{H_2O}^{melt}$ = 10.4 cm^3/mol).

Alternatively, the apparent large increase in $\bar{V}_{H_2O}^{melt}$ (Fig. 11A), obtained by Eqn. 4, with decreasing pressure results from the assumption that the activity coefficient of H_2O in melt, $\gamma_{H_2O}^{melt}$, is constant in the pressure ranges under consideration. The $\gamma_{H_2O}^{melt}$ may, however, vary with pressure. By assuming a constant $\bar{V}_{H_2O}^{melt}$ value, we can estimate the variations in $\gamma_{H_2O}^{melt}$ required to account for the variations in H_2O solubility. If we assume that the $\bar{V}_{H_2O}^{melt}$ = 10.4 cm^3/mol at P ≥ 0.8 GPa remains the same to lower pressure, the decrease in $\gamma_{H_2O}^{melt}$ with decreasing pressure at 1200°C relative to that at 0.8 GPa can be calculated (Fig. 11C). At 0.1 MPa the $\gamma_{H_2O}^{melt}$ is ~9% of the value at 0.8 GPa and increases as the pressure is increased.

The suggestion that $\bar{V}_{H_2O}^{melt}$ may not depend significantly on pressure is consistent with suggestions that the H_2O speciation equilibrium,

$$H_2O(melt) + O^{2-}(melt) = 2OH^-(melt), \quad (5)$$

does not appear to be significantly dependent on pressure (Zhang, 1993; Sowerby and Keppler, 1999). Therefore, even if the partial molar volume of water as molecular H_2O and as OH differ substantially, it would be surprising if pressure would have a major effect on the bulk $\bar{V}_{H_2O}^{melt}$ value. Furthermore, if the $\bar{V}_{H_2O}^{melt}$ remains constant (within experimental error) between 0.8 and 2.0 GPa, it would be surprising that the partial molar volume exhibits a strong pressure dependence at low pressures. Unless there are major changes in the H_2O solubility mechanism at lower pressures, the apparent large variations in $\bar{V}_{H_2O}^{melt}$ as shown in Figure 11A, therefore, are difficult to rationalize. There is not evidence at present for large changes on the solubility mechanisms of H_2O in silicate melts in this pressure range. We conclude, therefore, that the apparent large increase in $\bar{V}_{H_2O}^{melt}$ at low pressure, calculated from the H_2O solubility in melt, is an artifact of the assumption that $\gamma_{H_2O}^{melt}$ is constant in this pressure range.

4.5. Exsolution of H_2O from Hydrous Magma and Energy Release in Shallow Magma Chambers

In light of the discussion above, the high-pressure $\bar{V}_{H_2O}^{melt}$ values are, therefore, likely applicable to low pressures such as those experienced, for example, in felsic magma chambers in the uppermost portions of the crust (3- to 10-km depth; e.g., Rutherford et al., 1985; Foden, 1986; Skirius et al., 1990; Mandeville et al., 1996). The energy released by exsolution of H_2O from H_2O-saturated magmatic liquids as a function of pressure can also be estimated (Fig. 12). In deriving this estimate, the $\bar{V}_{H_2O}^{melt}$ values for dacite, andesite, and tholeiite melt at 1200°C from Fig. 8 were combined with the partial molar volume of H_2O in coexisting, silicate-saturated aqueous fluid as a function of pressure (Mysen and Acton, 1999). The partial molar volume of H_2O in silicate-saturated aqueous fluid is somewhat smaller than the molar

[4] Composition CS4A6 and the melt composition in CaO-Al_2O_3-SiO_2 from McMillan et al. (1986) are quite similar. Hence, results from these two compositions are discussed together in Figure 11A.

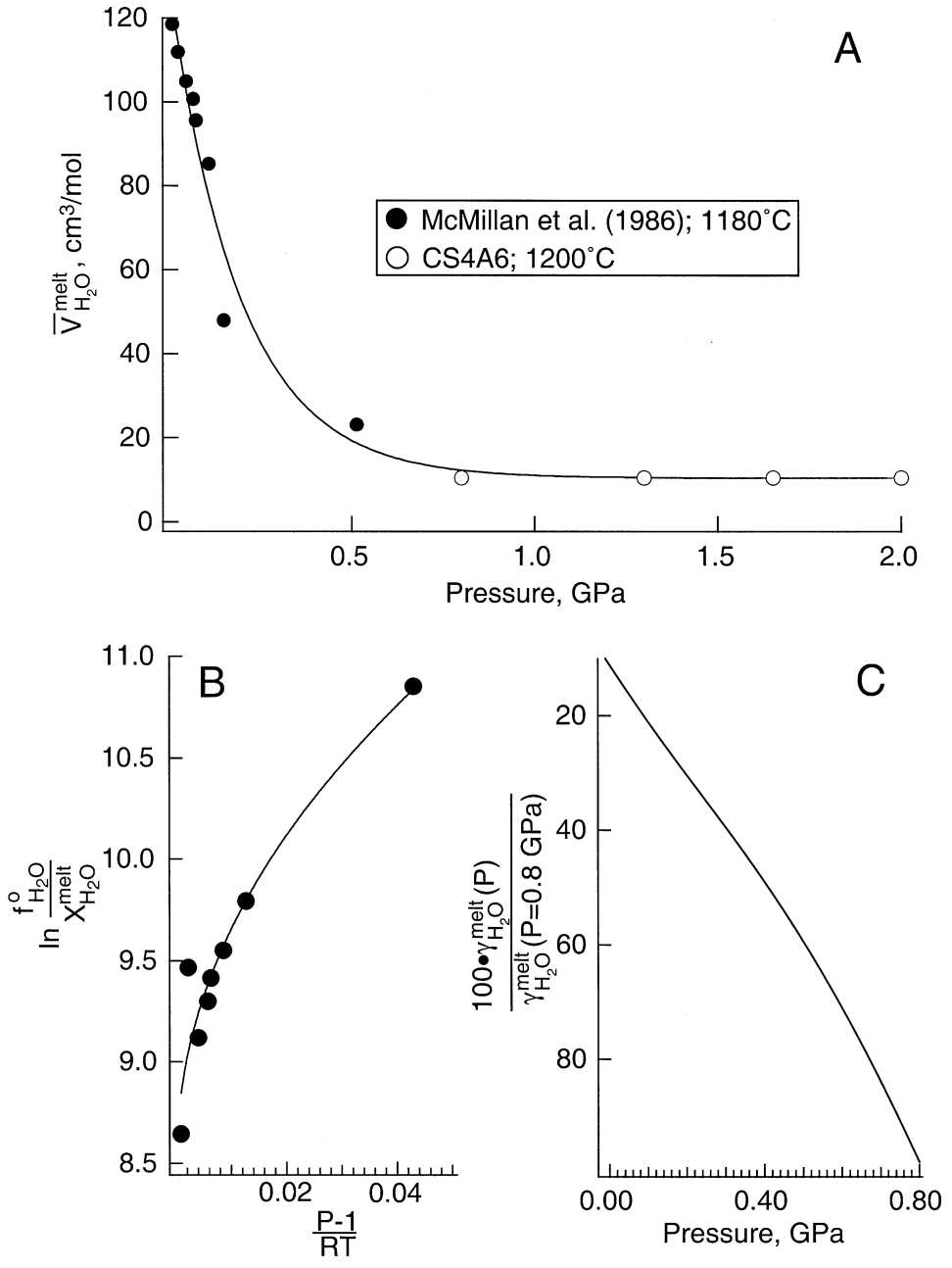

Fig. 11. (A) Apparent partial molar volume of H_2O, $\bar{V}^{melt}_{H_2O}$, from H_2O solubility of the CaO-Al_2O_3-SiO_2 melt composition used by McMillan et al. (1986) (NBO/T = 0.61, Al/(Al + Si) = 0.14) at 1180°C (solid symbols) and that for CS4A6 composition melt (open symbols) shown as a function of pressure. The line trough the data points is a fit to an exponential function. (B) Relationship between $\ln(f^{\circ}_{H_2O}/X^{melt}_{H_2O})$ and (P − 1)/RT at 1180°C from the H_2O solubility data of McMillan et al. (1986). Note that whereas the higher-pressure data for CS4A6 in Fig. 6 can be fitted to a straight line, the solubility data from McMillan et al. (1986) show distinct curvature. (C) Change in the activity coefficient of H_2O in melt at pressure, P < 0.8 GPa, $\gamma^{melt}_{H_2O}(P)$, relative to the activity coefficient of H_2O at 0.8 GPa, $\gamma^{melt}_{H_2O}$ (P = 0.8 GPa). See text for further discussion of these data and calculations.

volume of pure H_2O because of silicate dissolved in the aqueous fluid.[5] There is a small effect of silicate melt composition on this energy release because $\bar{V}^{melt}_{H_2O}$ depends on melt composition. The effect of melt composition is insignificant in the pressure regime of shallow felsic magma chambers but increases with increasing pressure. Regardless of details of the magma composition, in the pressure range of shallow felsic magma chambers, the energy release is approximately 1.5×10^8 erg/g H_2O exsolved from the magma to a coexisting aqueous fluid at the same pressure.

[5] This volume difference decreases with decreasing pressure because the silicate solubility decreases with decreasing pressure (Mysen and Acton, 1999; Mysen and Wheeler, 2000b).

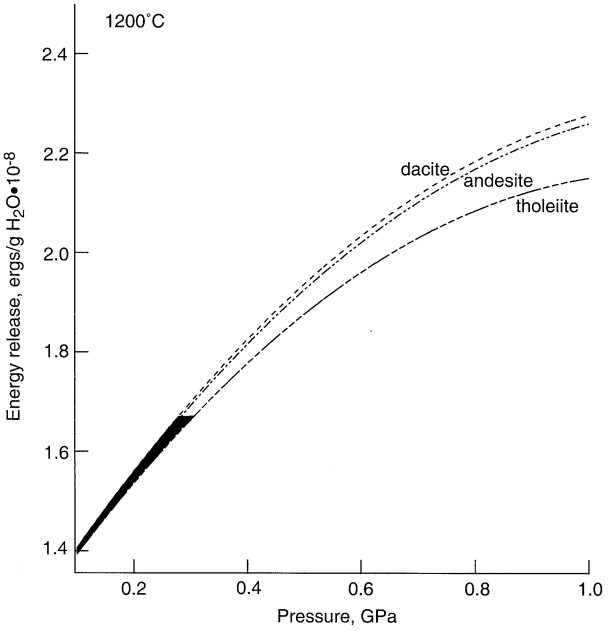

Fig. 12. Energy release per gram of H_2O exsolved from hydrous magma into silicate-saturated aqueous fluid as a function of pressure for the three melt compositions indicated (dacite, andesite, and tholeiite; Table 5). Shaded area denotes the pressure range typical for shallow dacitic magma chambers. See text for further discussion.

Acknowledgments—This research was conducted with partial support from NSF grant EAR-9901886. Reviews by two anonymous reviewers and Bruno Scaillet materially improved the manuscript. A portion of this work was conducted while I was in residence at the Institut de Physique du Globe de Paris, France. Their hospitality during this stay is greatly appreciated.

Associate editor: C. Romano

REFERENCES

Behrens H. and Cantos N. (2001) the effect of anhydrous composition on water solubility in granites melts. *Amery Mineral* **86,** 14–20.

Boettcher A. L. (1984) The system SiO_2-H_2O-CO_2: Melting solubility mechanisms of carbon and liquid structure to high pressures. *Am. Mineral.* **69,** 823–834.

Bohlen S. R., Boettcher A. L., and Wall V. J. (1982) The system albite-H_2O-CO_2: A model for melting and activities of water at high pressures. *Am. Mineral.* **67,** 451–462.

Boyd F. R. and England J. L. (1960) Apparatus for phase equilibrium measurements at pressures up to 50 kilobars and temperatures up to 1750°C. *J. Geophys. Res.* **65,** 741–748.

Burnham C. W. and Jahns R. H. (1962) A method for determining the solubility of water in silicate melts. *Am. J. Sci.* **260,** 721–745.

Burnham C. W. and Davis N. F. (1971) The role of H_2O in silicate melts. I. P-V-T relations in the system $NaAlSi_3O_8$-H_2O to 10 kilobars and 1000C. *Am. J. Sci.* **270,** 54–79.

Carroll M. R. and Blank J. G. (1997) The solubility of H_2O in phonolitic melts. *Am. Mineral.* **82,** 549–556.

Chayes F. (1975) Average composition of the commoner cenozoic volcanic rocks. *Carnegie Inst. Wash. Year Book* **74,** 547–549.

Dingwell D. B., Holtz F., and Behrens H. (1997) The solubility of H_2O in peralkaline and peraluminous granitic melts. *Am. Mineral.* **82,** 434–437.

Dingwell D. B., Hess K.-U., and Romano C. (1998) Viscosity data for hydrous peraluminous granitic melts: Comparison with the metaluminous model. *Am. Mineral.* **83,** 236–239.

Dixon J. E. and Stolper E. M. (1995) An experimental study of water and carbon dioxide solubilties in mid-ocean ridge basaltic liquids. Part II: Applications to degassing. *J. Petrol.* **36,** 1633–1646.

Eggler D. H. and Rosenhauer M. (1978) Carbon dioxide in silicate melts. II. Solubilities of CO_2 and H_2O in $CaMgSi_2O_6$ (diopside) liquids and vapors at pressures to 40 kb. *Am. J. Sci.* **278,** 64–94.

Eggler D. H. and Kadik A. A. (1979) The system $NaAlSi_3O_8$-H_2O-CO_2: I. Compositional and thermodynamic relations of liquids and vapors coexisting with albite. *Am. Mineral.* **64,** 1036–1049.

Eichelberger J. C. and Westrich H. R. (1981) Magmatic volatiles in explosive rhyolitic eruptions. *Geophys. Res. Lett.,* 757–760.

Foden J. (1986) The petrology of the Tambora volcano, Indonesia: A model for the 1815 eruption. *J. Volc. Geotherm. Res.* **27,** 1–41.

Gaetani G. A., Grove T. L., and Bryan W. B. (1993) The influence of water on the petrogenesis of subduction-related igneous rocks. *Nature* **365,** 332–334.

Goranson R. W. (1936) Silicate-water systems: The solubility of water in albite-melt. *Trans. Am. Geophys. Union* **17,** 257–259.

Haar L., Gallagher J. S., and Kell G. S. (1984) *Steam Tables: Thermodynamic and Transport Properties and Computer Programs for Vapor and Liquid States of Water in SI Units*. Hemisphere.

Hamilton D. L., Burnham C. W., and Osborn E. F. (1964) The solubility of water and the effects of oxygen fugacity and water content on crystallization of mafic magmas. *J. Petrol.* **5,** 21–39.

Hamilton D. L. and Oxtoby S. (1986) Solubility of water in albite melt determined by the weight loss method. *J. Geol.* **94,** 616–630.

Hodges F. N. (1974) The solubility of H_2O in silicate melts. *Carnegie Inst. Wash. Year Book* **94,** 251–255.

Holtz F., Behrens H., Dingwell D. B., and Johannes W. (1995) H_2O-solubility in haplogranitic melts: Compositional, pressure, and temperature dependence. *Am. Mineral.* **80,** 94–108.

Holtz F., Scaillet B., Behrens H., Schulze F., and Pichavant M. (1996) Water contents of felsic melts: Application to the rheological properties of granitic magmas. *The Third Hutton Symposium on the Origin of Granites and Related Rocks* In: (eds. M. Brown, P. A. Candela, D. L. Peck, W. E. Stephens, R. J. Walker, and E. A. Zen), 57–64. Geological Society of America.

Holtz F., Roux J., Ohlhorst S., Behrens H., and Schulze F. (1999) The effects of silica and water on the viscosity of hydrous quartzofeldspathic melts. *Am. Mineral.* **84,** 27–36.

Kress V. C. and Carmichael I. S. E. (1991) The compressibility of silicate liquids containing Fe_2O_3 and the effect of composition, temperature, oxygen fugacity and pressure on their redox states. *Contrib. Mineral. Petrol.* **108,** 92–92.

Kushiro I. (1972) Effect of water on the composition of magmas formed at high pressures. *J. Petrol.* **13,** 311–334.

Kushiro I. (1976) A new furnace assembly with a small temperature gradient in solid-media, high-pressure apparatus. *Carnegie Inst. Wash. Year Book* **75,** 832–833.

Kushiro I. (1978) Density and viscosity of hydrous calc-alkalic andesite magma at high pressure. *Carnegie Inst. Wash. Year Book* **77,** 675–678.

Kushiro I. (1990) Partial melting of mantle wedge and evolution of island arc crust. *J. Geophys. Res.* **95,** 15929–15939.

Lange R. A. and Carmichael I. S. E. (1987) Densities of Na_2O-K_2O-CaO-MgO-Fe_2O_3-Al_2O_3-TiO_2-SiO_2 liquids: New-measurements and derived partial molar properties. *Geochim. Cosmochim. Acta* **51,** 2931–2946.

Mandeville C. W., Carey S., and Sigurdsson H (1996) Magma mixing, fractional crystallization and volatile degassing during the 1883 eruption of Krakatau Volcano, Indonesia. *J. Volc. Geotherm. Res.* **74(3–4),** 243–274.

McMillan P., Peraudeau G., Holloway J. R., and Coutures J.-P. (1986) Water solubility in calcium aluminosilicate melt. *Contr. Mineral. Petrol.* **94,** 178–182.

Merzbacher C. I. and White W. B. (1991) The structure of alkaline earth aluminosilicate glasses as determined by vibrational spectroscopy. *J. Non-Cryst. Solids.* **130,** 18–34.

Mysen B. O. (1987) Magmatic silicate melts: Relations between bulk composition, structure and properties. *Magmatic Processes: Physiochemical Principles* In: (ed. B. O. Mysen), 375–399. Special Publication. Geological Society of America.

Mysen B. O. (1995) Experimental, in-situ, high-temperature studies of properties and structure of silicate melts relevant to magmatic temperatures. *Eur. J. Mineral.* **7,** 745–766.

Mysen B. O. (2002) Solubility of alkaline earth and alkali aluminosilicate components in aqueous fluids in the Earth's upper mantle. *Geochim. Cosmochim. Acta* **66**(13), 2421–2438.

Mysen B. O. and Boettcher A. L. (1975) Melting of a hydrous mantle. II. Geochemistry of crystals and liquids formed by anatexis of mantle peridotite at high pressures and high temperatures as a function of controlled activities of water, hydrogen and carbon dioxide. *J. Petrol.* **16,** 549–590.

Mysen B. O. and Virgo D. (1986a) Volatiles in silicate melts at high pressure and temperature. 1. Interaction between OH groups and Si^{4+}, Al^{3+}, Ca^{2+}, $Na^{+}$and H^{+}. *Chem. Geol.* **57,** 303–331.

Mysen B. O. and Virgo D. (1986b) Volatiles in silicate melts at high pressure and temperature, 2: Water in melts along the join NaAlO2-SiO2 and a comparison of solubility mechanisms of water and fluorine. *Chem. Geol,* **57(3–4),** 333–358.

Mysen B. O. and Acton M. (1999) Water in H_2O-saturated magma–fluid systems: Solubility behavior in K_2O-Al_2O_3-SiO_2-H_2O to 2.0 GPa and 1300°C. *Geochim. Cosmochim. Acta* **63,** 3799–3816.

Mysen B. O. and Wheeler K. (2000a) Solubility Behavior of Water in Haploandesitic. Melts at high Pressure and high Temperature. *Am. Mineral.* **85,** 1128–1142.

Mysen B. O. and Wheeler K. (2000b) Alkali aluminosilicate-saturated aqueous fluids in the Earth's upper mantle. *Geochim. Cosmochim. Acta* **64,** 4243–4256.

Nowak M. and Behrens H. (1995) The speciation of water in haplogranitic glasses and melts by in-situ, near-infrared spectroscopy. *Geochim. Cosmochim. Acta* **59,** 3445–3450.

Nowak M. and Behrens H. (1997) An experimental investigation on diffusion of water in haplogranitic melts. *Contrib. Mineral. Petrol.* **126,** 365–376.

Ochs F. A. and Lange R. A. (1997) The partial molar volume, thermal expansivity, and compressibility of H_2O in $NaAlSi_3O_8$ liquid: New measurements and an internally consistent mode. *Contrib. Mineral. Petrol.* **129,** 155–165.

Osborn E. F. and Muan A. (1960) *Phase Equilibrium Diagrams of Oxide Systems, Plate 2: The System CaO-Al_2·O_3-SiO_2.* American Ceramic Society.

Paillat O., Elphick E. C., and Brown W. L. (1992) The solubility behavior of H_2O in $NaAlSi_3O_8$ melts: A re-examination of Ab-H_2O phase relationships and critical behavior at high pressure. *Contrib. Mineral. Petrol.* **112,** 490–500.

Richet P. and Neuville D. R. (1992) Thermodynamics of silicate melts: Configurational properties. *Thermodynamic Data: Systematics and Estimation,* Vol. 10 In: (ed. S. K. Saxena), 132–161. Springer.

Richet P. and Polian A. (1998) Water as a dense icelike component in silicate glasses. *Science* **281,** 396–398.

Romano C., Poe B. T., Mincione V., Hess K. U., and Dingwell D. B. (2001) The viscosities of dry and hydrous $XAlSi_3O_8$ (X= Li, Na, K, $Ca_{0.5}$, $Mg_{0.5}$) melts. *Chem. Geol.* **174,** 115–132.

Rutherford M. J., Sigurdsson H., Carey S., and Davis A. (1985) The May 18, 1980, eruption of Mount St. Helens: 1—Melt composition and experimental phase equilibria. *J. Geophys. Res.* **90,** 2929–2947.

Schulze F., Behrens H., Holtz F., Roux J., and Johannes W. (1996) The influence of H_2O on the viscosity of haplogranitic melt. *Am. Mineral.* **81,** 1155–1165.

Shen A. and Keppler H. (1995) Infrared spectroscopy of hydrous silicate melts to 1000°C and 10 kbar: Direct observation of H_2O speciation in a diamond cell. *Am. Mineral.* **80,** 1335–1338.

Skirius C. M., Peterson J. W., and Anderson A. T. (1990) Homogenizing rhyolitic glass inclusions from the Bishop Tuff. *Am. Mineral.* **75,** 1381–1398.

Sowerby J. R. and Keppler H. (1999) Water speciation in rhyolitic melt determined by in-situ infrared spectroscopy. *Am. Mineral.* **84,** 1843–1849.

Stalder R., Ulmer P., Thompson A. B., and Gunther D. (2000) Experimental approach to constrain second critical endpoints in fluid/silicate systems: Near-solidus fluids and melts in the system abite-H_2O. *Am. Mineral.* **85,** 68–77.

Toplis M. J. (1998) Energy barriers associated with viscous flow and the prediction of glass transition temperatures of molten silicates. *Am. Mineral.* **83,** 480–490.

Woods A. W. (1988) The fluid dynamics and thermodynamics of eruption columns. *Bull. Volcan.* **50,** 169–193.

Zhang Y. (1993) Pressure dependence of the speciation of water in rhyolitic glasses. *EOS* **74,** 631.

Zhang Y., Stolper E. M., and Wasserburg G. J. (1991) Diffusion of water in rhyolitic glasses. *Geochim. Cosmochim. Acta* **55(2),** 441–456.